Journal of Materials Chemistry B

PAPER

View Article Online
View Journal | View Issue

Cite this: J. Mater. Chem. B, 2015, 3, 144

In vivo analysis of the size- and time-dependent uptake of $NaYF_4$:Yb,Er upconversion nanocrystals by pumpkin seedlings†

J. Nordmann,[a] S. Buczka,[b] B. Voss,[a] M. Haase*[a] and K. Mummenhoff*[b]

Received 11th September 2014
Accepted 23rd October 2014

DOI: 10.1039/c4tb01515k

www.rsc.org/MaterialsB

We have investigated the kinetics of the uptake and the translocation of nanoparticles in plants. Nearly monodisperse $NaYF_4$:Yb,Er nanocrystals were used, either spherical particles with a diameter of 14 nm or nanorods with a length of 41 nm and a diameter of 22 nm. After watering pumpkin seedlings (*Cucurbita maxima*) with aqueous colloidal solutions of the particles, intact nanocrystals in the plants were detected *in vivo* by exciting their upconversion luminescence with a near infrared laser diode (978 nm). The particle concentration in different plant parts was determined by X-ray fluorescence spectroscopy (XRF), making use of the high sensitivity of Yttrium in XRF measurements and its low natural abundance in plants. The results show a fast uptake and translocation of the nanoparticles in all plant organs within three hours. The smaller particles move in the plants faster than the larger ones.

1 Introduction

The rapid progress in the development of nanoparticles (NPs) results in an increasing use of these materials in daily-life products. NPs of some materials are already produced on an industrial scale in quantities of several thousand tons per year (TiO_2: 3 kt per annum; SiO_2: 5.5 kt per annum; ZnO: 550 t per annum; carbon nanotubes: 300 t per annum; FeO_x: 55 t per annum; CeO_x: 55 t per annum; AlO_x: 55 t per annum; Ag: 55 t per annum; fullerenes: 0.6 t per annum; quantum dots: 0.6 t per annum).[1] These products are used, for instance, for UV protection in cosmetics and creams (TiO_2, ZnO), as white pigments in the paint and coatings industry (TiO_2, ZnO, CeO_x) and as antimicrobial additives in paints and clothes (Ag).[2,3] The increasing production rates of NPs and the general interest in nanotechnology have also promoted new research activities on the interaction of NPs with the environment including living organisms. In fact, the gap between technological progress and the investigation of possible environmental hazards and other safety issues concerning NPs has been reported to present a big challenge for the (scientific) community.[4] Therefore, several research initiatives focussing on potential environmental risks of NPs started in the last few years, but concentrate mainly on animal and water ecosystems like microorganisms, aquatic invertebrates and various fish species.[4–7] On the contrary, there are only very few studies on the interaction of NPs with plants and their environment, even though plants as primary producers are the base component of all ecosystems and may therefore act as the "entrance door" for the introduction of NPs into organism communities and ecosystems *via* the different food chains.[4,8–18] In these studies it was shown that dispersible NPs of some materials can enter plants as intact particles [$Ni(OH)_2$, ZnO, CeO_2, Cu, Ag, Al, Fe_3O_4, $NaYF_4$:Yb,Er, carbon nanotubes and fullerenes] whereas NPs of other materials slowly release ions which subsequently enter the plant (*e.g.*, Ag^+, Al^{3+}, Zn^{2+}, Cu^{2+}).[10,12,15,16,19–28] However, only for fullerols, Fe_3O_4, $Ni(OH)_2$ and Cu NPs conclusive studies exist on the absorption and movement of NPs into upper organs of living plants.[18]

Optical methods are commonly used in biology but in the case of plants the presence of plant pigments with strong absorption bands in the UV and visible range make it difficult to excite luminescent NPs *in vivo*. This problem can be greatly relaxed by using NPs showing energy transfer upconversion emission. In these materials, two or more near-infrared photons (NIR photons, wavelength around 974 nm) are sequentially absorbed by Yb^{3+}-sensitizer ions followed by rapid transfer of their energy to a nearby activator ion (Er^{3+}, Tm^{3+}, Ho^{3+}).[29] As the energy of two or more NIR photons is transferred to one ion, each activator ion reaches a highly excited state resulting in luminescence emission in the visible range, that is at shorter wavelengths than the excitation wavelength. The highest quantum efficiency of all upconversion materials known today is observed for the hexagonal phase of $NaYF_4$ doped with Yb^{3+} and Er^{3+}. Quantum yields of up to 20% were measured for

[a]University of Osnabrück, Institute of Chemistry, Barbarastraße 7, 49076 Osnabrück, Germany. E-mail: markus.haase@uos.de

[b]University of Osnabrück, Department of Biology/Chemistry, Botany section, Barbarastraße 11, 49076 Osnabrück, Germany. E-mail: Mummenhoff@Biologie.Uni-Osnabrueck.DE

† Electronic supplementary information (ESI) available: XRD data (Fig. S1), histogram (Fig. S2), DLS measurements (Fig. S3), long time DLS measurements (Fig. S4), IR spectra (Fig. S5), emissions spectra (Fig. S6), further XRF data (Fig. S7; Tables S1 and S2) and experimental procedures (Fig. S8 and S9). See DOI: 10.1039/c4tb01515k

microcrystalline $NaYF_4$:Yb,Er and of 0.005–0.30% for nanocrystalline materials.[30,31] Currently, NPs of this material are intensively investigated as a new class of luminescent markers in diagnostics because they provide several advantages over classic luminescent material. The excitation wavelength is located in the "optical window" of biological systems (NIR from 800 to 1050 nm) and therefore assures excitation of NPs even in deeper tissue regions. Furthermore, excitation in the NIR leads to negligible autofluorescence from the biological material in the visible range, and can also be used for *in vivo* studies. The inorganic upconversion nanocrystals are resistant against photobleaching, display no blinking and have a high photostability.[29,32] Due to the line emission of Er^{3+}, which resembles an optical fingerprint of the upconversion luminescent nanoparticles (UCNP), the particles can easily be identified by luminescence microscopy. The detection of upconversion emission also proves that the particles have not dissolved, since the upconversion process is only efficient as long as the lanthanide ions are part of a rigid crystal lattice with low phonon energy. In addition, the high atomic mass of the rare earth ions results in a high contrast of the particles in transmission electron microscopy. The very low natural abundance of yttrium in plants and its high sensitivity in X-ray fluorescence spectroscopy (XRF) allow (i) a mass determination of Yttrium on the nanogram scale *via* XRF and, therefore, (ii) also the detection of UCNPs in biological tissues. A combination of these methods therefore enables a fast and simple detection and quantification of UCNPs in fresh plant objects without extensive preparation procedures. Because of these benefits UCNP were used as optical marker system in prokaryotes and animals, but apart from our previous work only one study used UCNPs in plants.[33–36]

The mechanisms of uptake and translocation of nanoparticles in plants have not been intensively investigated yet but it was suggested that surface properties, particle size, solubility and the tendency to form agglomerates are important factors.[8] Very little is known about the short- and mid-term kinetics of the uptake and distribution in plants as all studies analysed NP uptake after an incubation time of 5–20 days.[9,10,37] In our previous study we detected the uptake of cubic phase $NaYF_4$:Yb,Er-UCNPs (functionalized with L-hydroxyethane-1,1-diphosphonic acid) into aerial roots of orchids already 10 minutes after incubation, and after six days UCNPs-signals were observed in the vascular cylinder of the stem and in the leaves.[35] In this study, however, polydisperse UCNPs (mean crystallite size 45 nm, XRD; hydrodynamic radii 40–150 nm, DLS) were used and a quantitative analysis of the particle concentration was not performed.[5] In the current study we used monodisperse hexagonal phase UCNPs with well-defined sizes and higher luminescence efficiency as a model system to investigate the size-dependent uptake and translocation of NPs in hydroponically cultivated pumpkin plants (*Cucurbita maxima*). This test design represents a simple system to study the uptake and translocation of NPs by optical analysis *in vivo* and to quantify the particle concentration in all plant organs by X-ray fluorescence spectroscopy (XRF) without complex preparation.

2 Experimental section

2.1 Nanoparticle synthesis

Small purified α-$NaYF_4$-particles were used as precursors for the synthesis of larger β-$NaYF_4$-particles as published by Mai *et al.*[38,39] We prepared the α-phase precursor particles by reacting rare-earth oleates, sodium oleate (82%, Alfa Aesar) and ammonium fluoride (98%, Sigma-Aldrich) in a solvent mixture of oleic acid (90%, Alfa Aesar) and octadecene (90%, Alfa Aesar).[40–43] In the present paper a hot-injection method was used to convert the α-phase particles into larger β-phase particles.

Synthesis of metal oleates. A solution of 60 mmol rare-earth chlorides (46.8 mmol YCl_3, 12.0 mmol $YbCl_3$ and 1.2 mmol $ErCl_3$ in the case of α-$NaYF_4$:Yb,Er particles and 60 mmol $GdCl_3$ in the case of α-$NaGdF_4$ particles used for shell growth; all 99.9%, Treibacher Industrie AG) in 80 mL of water was combined with 120 mL ethanol and 210 mL hexane. Sodium oleate (180 mmol) was added, dissolved under stirring and the resulting mixture was heated to reflux for 14 h. After cooling to room temperature, the metal oleates were isolated as waxy solid by separating the upper organic phase with a separation funnel and removing the organic solvent with a rotavap.

Synthesis of 3–4 nm α-phase precursor particles. Small α-$NaYF_4$:Yb,Er particles were prepared by combining 55 mmol of rare-earth oleates, 137.5 mmol of sodium oleate, (*i.e.*, a 2.5 fold excess of sodium), 137.5 mL of oleic acid and 137.5 mL of octadecene and heating the mixture to 100 °C under vacuum (1 mbar) and stirring. After 60 minutes at 100 °C the Schlenk-line was switched to nitrogen atmosphere and 220 mmol of solid ammonium fluoride were added to the clear yellowish solution under nitrogen flow. Directly thereafter, the apparatus was cycled three times between vacuum and nitrogen atmosphere, applying vacuum for only 5 seconds in each cycle. Next, the reaction mixture was heated to 240 °C under nitrogen atmosphere and kept at this temperature for 90 minutes. After cooling to room temperature the volume of the solution was doubled by the addition of ethanol, leading to precipitation of the nanoparticles. The particles were separated by centrifugation (5 minutes, 3260 g), re-dispersed in 10 mL hexane and again precipitated by adding 40 mL ethanol. After centrifugation the precipitate was dried at 80 °C over night. The yield of nanoparticles exceeds 86%. For the calculation of the yield the high amount of volatilizable organic material in the precipitate was taken into account (approx. 45% mass loss in thermogravimetric measurements under helium atmosphere).

Small α-$NaGdF_4$ particles were prepared similarly by combining 50 mmol gadolinium oleate, 400 mmol NaF, 250 mL oleic acid and 250 mL octadecene in a 1 l three neck flask and heating the mixture under vacuum (1 mbar) and stirring to 100 °C. After 60 minutes at 100 °C the Schlenk-line was switched to nitrogen atmosphere and the solution heated at 200 °C for one hour. After cooling to room temperature excess NaF was removed by centrifugation (5 minutes, 3260 g) and the clear supernatant was treated as described for the α-$NaYF_4$:Yb,Er precursor particles.

Preparation of 12 nm β-$NaYF_4$:Yb,Er core particles *via* hot-injection synthesis. A 500 mL three necked round bottom flask with attached thermosensor, Miethke-type dropping funnel and reflux condenser was used for the reaction. The three-neck flask was charged with 150 mL of oleic acid and 150 mL of octadecene. A discharge cock connected to a small flask was introduced between the condenser and the three neck flask. Low-boiling constituents were distilled off *via* the discharge cock by heating the solvent mixture for 60 minutes at 100 °C under vacuum and stirring. Thereafter the Schlenk-line was switched to nitrogen atmosphere and the solvent was heated to 330 °C.

In a similar setup with a smaller three-necked round bottom flask 10 mmol of α-$NaYF_4$:Yb,Er-precursor particles, 25 mL of oleic acid and 25 mL of octadecene were heated at 100 °C under vacuum and stirring for 60 minutes. During this time a small amount of low-boiling liquid distilled off. After cooling to room temperature under nitrogen atmosphere, the solution was transferred into the dropping funnel of the larger setup. The solution of the precursor particles in the dropping funnel was rapidly added (7 mL s^{-1}) to the hot solvent. After 60 minutes at 320 °C the reaction mixture was cooled to room temperature and the product was isolated as described above for the precursor particles.

Preparation of 14 nm β-$NaYF_4$:Yb,Er/$NaGdF_4$ core/shell particles *via* hot-injection synthesis. The procedure was analogous to the hot-injection synthesis given above except that the oleic acid/octadecene solvent mixture was replaced by a solution of the 12 nm β-$NaYF_4$:Yb,Er core particles in oleic acid and octadecene. The latter solution was prepared by re-dispersing 5 mmol β-$NaYF_4$:Yb,Er core particles in 50 mL oleic acid and 50 mL octadecene under vacuum at 100 °C. In a second setup 2.5 mmol α-$NaGdF_4$ precursor particles were dispersed in 12.5 mL oleic acid and 12.5 mL octadecene and heated under vacuum to 100 °C for 60 minutes. Thereafter, the solution for the α-$NaGdF_4$ shell material was transferred into the dropping funnel of the first setup and added slowly (1 drop per second) to the solution of the core particles at 320 °C under nitrogen atmosphere. After the whole solution had been added the reaction mixture was kept for additional five minutes at 320 °C. Subsequently, the setup was allowed to cool down to room temperature and the product was isolated as described above for the precursor particles.

Synthesis of β-$NaYF_4$:Yb,Er nanorods (22 × 41 nm) *via* heat-up synthesis. 50 mmol of rare earth oleates and 50 mmol of sodium oleate were dissolved in 50 mL oleic acid and 50 mL octadecene by stirring the mixture at 100 °C under vacuum (1 mbar). After 90 minutes, the Schlenk-line was switched to nitrogen atmosphere and 200 mmol of solid ammonium fluoride were added to the clear yellowish solution under nitrogen flow (100 °C). Directly thereafter, the apparatus was cycled three times between vacuum and nitrogen atmosphere, applying vacuum for only 5 seconds in each cycle. Finally, the reaction mixture was heated to 320 °C under nitrogen atmosphere and kept at this temperature for 90 minutes. The product was isolated as described above for the precursor particles.

2.2 Ligand exchange and functionalization of the NP with L-hydroxyethane-1,1-diphosphonic acid (HEDP)

0.21 g of NP were dispersed in 21 g chloroform and mixed with a solution containing 0.226 g HEDP and 22.65 g ethanol. After stirring the solution for 20 hours at room temperature, 21 mL of water were added and the reaction stirred for additional 15 minutes. The upper water phase containing the NP were collected by using a separating funnel and transferred to a 250 mL Erlenmeyer flask. Next, the pH value of the aqueous solution was adjusted to pH 6 by adding the sodium salt of HEDP. The ethanol was subsequently removed with a rotavap (100 mbar, 40 °C). For further purification the solution was dialysed three times against 1200 mL of a 1 wt% Na–HEDP solution. The 1 wt% Na–HEDP solution was exchanged after one and three hours.

2.3 Plant tests

Cucurbita maxima (Jaune Gros de Paris, Quedlinburger-Saatgut GmbH, Aschersleben) seeds were sterilized by treating them with a 10% H_2O_2-solution for 30 minutes. Subsequently, the seeds germinated on moist filter paper at 30 °C in the dark. After three days the seedlings were transferred to a crystallising dish which contained 800 mL of a nutrient solution. The dish was coated on the outer site with black sticky tape and was equipped with an air pump. The plants were fixed over the nutrient solution, so that only the roots were in direct contact to the nutrient solution (see Fig. S8†). The nutrient solution was changed after three days of acclimatization. The plants were grown in a greenhouse at 25 °C, 40% relative humidity, 18/6 day–night cycle and 4700 lux (400 W sodium vapour lamp). For hydroponic plant cultivation a 0.1% nutrient solution (Hakaphos-Rot, COMPO, Münster) was used which contained 0.1 wt% HEDP functionalized NP. Before use, the pH of the solution was adjusted to 6.5 with 0.1 M KOH. After different periods of time plants were collected, rinsed thoroughly with water and analysed for NP uptake and translocation. The upconversion emission of the nanoparticles inside the plants was excited by slowly moving the beam of a NIR laser diode over the plant (978 nm laser diode with 5 W cw-power, laser diode connected to a glass-fiber with collimator, beam diameter of 0.25 cm after the collimator). During excitation with the laser diode, images of the luminescing plants were taken with a standard digital camera using an exposure time of 30 s. The camera was equipped with an optical filter blocking NIR light between 850 nm and 1150 nm. Subsequently, the plants were cut into sections representing different plant organs such as root, root collar (lower hypocotyl), upper hypocotyl, cotyledons (divided into leaf margin and leaf blade), primary leaf (first true leaf that emerges on a plant following the cotyledons) and foliage leaves (adult leaves). These sections were analyzed by XRF spectroscopy (see Fig. S9†).

2.4 Instrumentation

XRD measurements were performed with an X'pert-Plus System (Panalytical), TEM-images were recorded with a JEM 2100

transmission electron microscope (JEOL) operated at 200 kV. Luminescence spectra of the samples were recorded with a Fluorolog 3-22 spectrometer (Jobin-Yvon) using a 978 nm cw-laser diode for excitation. For DLS-measurements a Nanosizer (Malvern) was used. Laser scanning microscopy was performed with the LSM Zeiss 510 meta The samples were excited with a titan sapphire laser with pulse width in the femtosecond range.

3 Results and discussion

3.1 Characterisation UCNPs

$NaYF_4$:Yb,Er/$NaGdF_4$ core/shell particles and $NaYF_4$:Yb,Er nanorods, both of the hexagonal phase (β-phase) and with narrow size-distribution, were synthesized by heating small (2–4 nm) particles of the cubic α-phase as precursors (sacrificial particles) in oleic acid/octadecene mixtures as solvent. Depending on the reaction conditions either spherical 14 ± 1.4 nm (10%) core/shell particles (Fig. 1a, TEM; Fig. S1a,† XRD; Fig. S2a,† histogram) or nanorods (Fig. 1b, TEM; Fig. S1b,† XRD; Fig. S2b,† histogram) with a length of 41 ± 2.3 nm (5%) in *c*-axis and a diameter of 22 ± 1.8 nm (8%) in *a*-axis were obtained. The synthesis route based on sacrificial particles yields β-$NaREF_4$ particles in gram amounts. As-prepared UCNPs bear oleic acid ligands on their surface and are therefore only dispersible in nonpolar solvents. After ligand exchange with the negatively charged L-hydroxyethane-1,1-diphosphonic acid (HEDP) the UCNPs become dispersible in water, and the resulting aqueous colloidal solutions are stable over weeks without agglomeration of the particles. Dynamic light scattering measurements (DLS) show the same particle size in solution before and after HEDP functionalization (see Fig. S3,† for long time DLS measurement see Fig. S4;† for IR spectra see Fig. S5†). HEDP was chosen as organic surface ligand because of its strong coordination to surface metal ions and since our earlier results have shown that HEDP functionalized α-$NaYF_4$:Yb,Er-NPs were taken up by plants.[35] The size of the particles was chosen to be lower (14 nm spherical particles) or larger (22 × 41 nm nanorods) than the maximum diameter of the pores in the walls (20 nm) of plant cells.[44] Seedlings of *Cucurbita maxima* were hydroponically grown in plain nutrient solution for six days. Thereafter the medium was exchanged by a nutrient solution containing 0.1 wt% of UCNPs functionalized with HEDP. The UCNP uptake was analysed *via* optical analysis and XRF spectroscopy after defined periods of time (optical analysis after 96 and 192 h; XRF analysis after 3, 6, 24, 72 and 120 h).

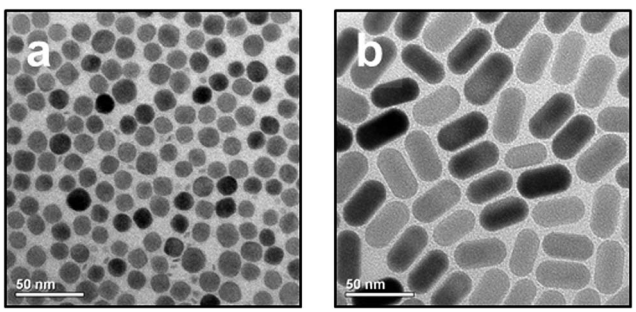

Fig. 1 TEM images of UCNPs. Spherical 14 nm β-$NaYF_4$:Yb,Er/$NaGdF_4$-core/shell particles (a) and 22 × 41 nm β-$NaYF_4$:Yb,Er nanorods (b) were used.

3.2 Qualitative *in vivo* analysis of UCNP uptake in *C. maxima*

Fig. 2 displays photographs of *C. maxima* seedlings taken eight days after incubation with HEDP functionalized 14 nm β-

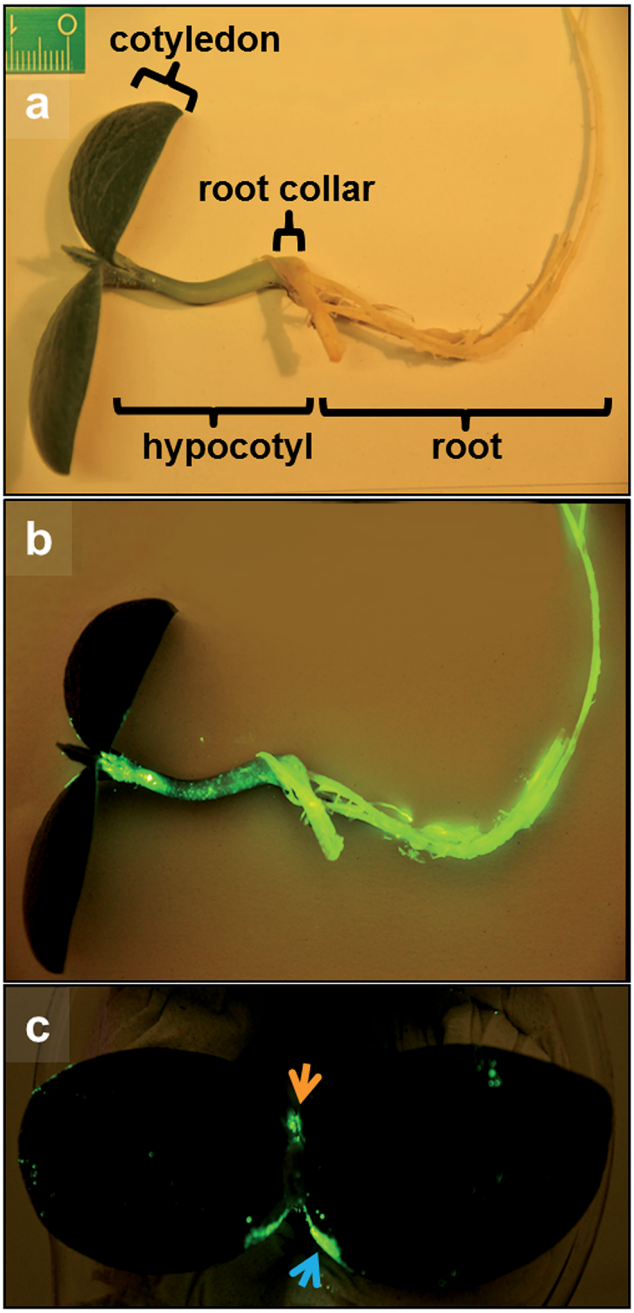

Fig. 2 *Cucurbita maxima* seedling hydroponically grown for eight days in a 0.1 wt% solution of HEDP functionalized 14 nm β-$NaYF_4$:Yb,Er/$NaGdF_4$ core/shell particles. (a) Seedling under daylight, (b) seedling under NIR excitation (980 nm, cw, 5 W, 30 s) and (c) top view of cotyledons under NIR excitation with strong UC luminescence at the leaf base (orange arrow) and margin (blue arrow).

$NaYF_4$:Yb,Er/$NaGdF_4$ core/shell particles. Irradiation with the light of a 980 nm laser diode results in the emission of the characteristic yellow-green Er^{3+} upconversion luminescence in the roots and in the upper plant organs (lower parts of Fig. 2). Strong signals of the UCNPs are observed also in the upper hypocotyl (stem parts of seedlings between cotyledons and root collar, Fig. 2) and the base and margin of the cotyledons (leaves of seedling). Fig. 2 clearly shows that the uptake of nanoparticles by plants can be identified *in vivo* due to the special optical properties of UCNP. The methodology is simple, very fast and reliable due to absence of any autofluorescence background of biological tissue. To identify the translocation route of the UCNPs in the plant we performed additional laser scanning microscopy (LSM) studies, thereby using excitation with a NIR laser at 974 nm. Fig. 3 shows a longitudinal section of the root collar (lower part of the hypocotyl representing the transition zone between the shoot and the root, Fig. 2) of a pumpkin seedling grown for four days in 0.1 wt% UCNP solution. In addition to the surface of the root collar, which was in direct contact with the UCNP solution, the fluorescence of the UCNPs is also detected in the tissues of the root collar. Isolated signals are detected in the parenchyma and concentrated signals along the axially elongated vascular tissue, which is responsible for long distance transport of water and solutes. Emission spectra of the signals from the vascular tissue clearly demonstrate the typical Er^{3+}-emission lines of the upconversion luminescence (see UCNPs emission spectra Fig. S6†).

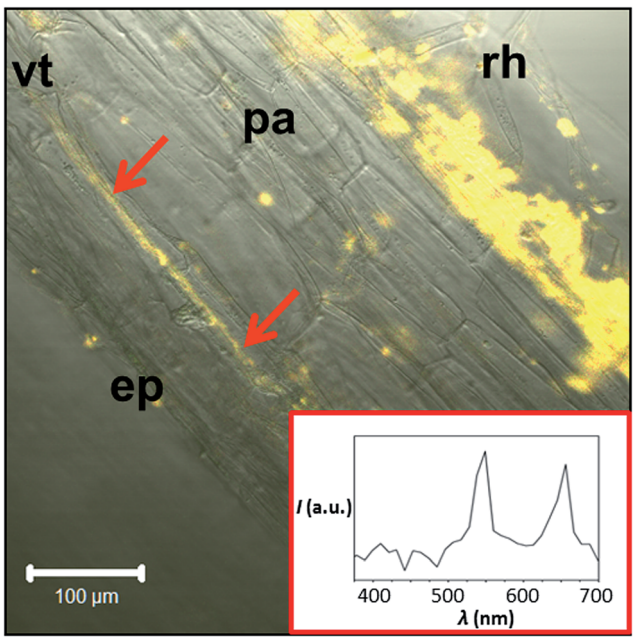

Fig. 3 Laser scanning microscopy (LSM) image of a longitudinal section of a *C. maxima* root collar after UCNP treatment for four days ($\lambda_{excitation}$: 974 nm; 0.6 W; $\lambda_{emission}$: 405–415 nm, 544–554 nm and 651–661 nm). The presence of β-$NaYF_4$:Yb,Er/$NaGdF_4$ core/shell UCNPs was verified by the emission spectra (inset) of the yellow signals (red arrows) showing the typical erbium lines of the UC emission. A continuous line of UCNP signals is found along the axially elongated vascular tissue (vt; red arrows). In addition, UCNPs are located in single parenchyma cells (pa) and at the root collar's surface (ep: epidermis; rh: root collar rhizoids).

3.3 Quantitative analysis of UCNP uptake in *C. maxima*

After proving the uptake of the UCNPs *via* the roots and their translocation to all plant organs by luminescence measurements we quantified the number of particles in each plant organ by X-ray fluorescence spectroscopy (XRF). At different times after incubation, plants were removed from the hydroponic setup and the roots were thoroughly rinsed to remove adhering NPs. Subsequently, the different plant organs, *i.e.*, root, upper hypocotyl and leaf, *i.e.*, cotyledons, primary leaf (first true leaf that emerges on a plant following the cotyledons) and foliage leaves (adult leaves) were cut off. A new blade used for every cut to avoid contamination with particles from earlier usage. Because of its special morphology the hypocotyl was cut further into root collar (= lower hypocotyl) and upper hypocotyl. For each sample, the number of UCNPs per (fresh) weight was measured by XRF as displayed in Fig. 4. The upper part of the figure (Fig. 4a) shows that the smaller 14 nm particles as well as the larger nanorods (22 × 41 nm) are present in all plant organs already 3 hours after incubation started. The highest UCNP concentrations are found in the roots. At early times, the concentration of the small particles exceeds the concentration of the larger nanorods in all upper plant organs. Three hours after the beginning of incubation, for instance, the concentration of the small spherical particles is by a factor of 9 higher in the upper hypocotyl and by a factor of 23 higher in the leaves (cotyledons, primary leaf and foliage leaf) than the concentration of the larger nanorods. The concentration difference between the smaller and larger particles, however, decreases with increasing time. Already after 120 hours similar concentrations are determined for nanorods and spherical particles in the leaves. Thus, the larger nanorods need more time than the smaller particles to achieve the same concentration in the leaf. Fig. 4b shows the concentrations of the UCNPs in two different areas of the leaves (cotyledons), *i.e.*, the leaf center (basis/blade) and the leaf margin. Again, the concentration of the small particles exceeds the concentration of the larger nanorods at early times. As in Fig. 4a, this concentration difference decreases with increasing time indicating that the larger nanorods need more time than the smaller particles to achieve the same concentration. Fig. 4b also shows that in the beginning of the experiment the concentration of the UCNPs is approximately the same in both cotyledon areas. After 120 hours, however, the particle concentration is almost seven (large UCNP) to nine (small UCNP) times higher at the leaf margin compared to the leaf basis/blade. This accumulation of particles at the leaf margin is observed for both particle sizes.

The XRF data showing the translocation of both particle sizes from the roots to the leaves are therefore in accord with the confocal laser-scanning microscopy images (Fig. 2) which indicate long distance transport *via* the vascular tissue of the root collar and the hypocotyl. Since the lowest UCNP concentration of small and large UCNPs was found in the upper hypocotyl, we conclude that the NP were taken up by the roots,

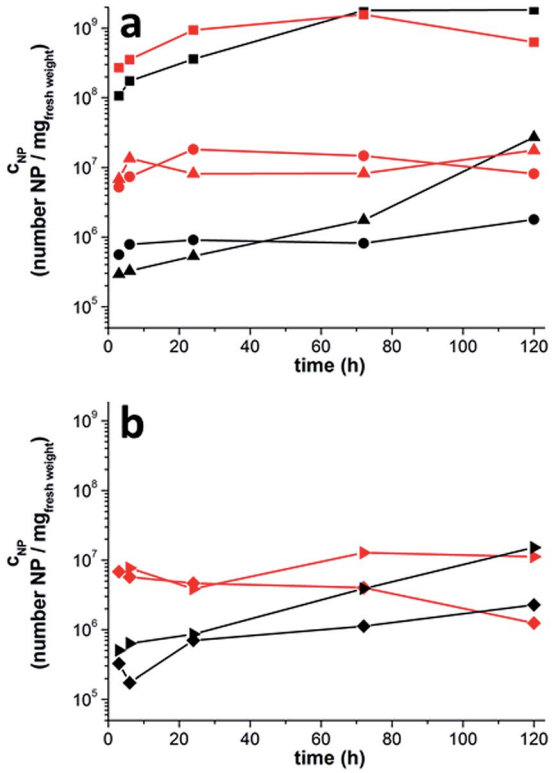

Fig. 4 Number of small UCNPs (14 nm, red) and larger UCNPs (nanorods 22 × 41 nm, black) per milligram fresh weight at different times after incubation (3, 6, 24, 72, 120 h). Part (a): particle concentrations in roots (■), upper hypocotyl (●) and leaves (▲). Part (b): particle concentrations in different cotyledon regions (► leaf margin; ◆ leaf base and leaf blade). The number of UCNPs was determined by X-ray fluorescence analysis.

transported *via* the vascular tissue, passed through the hypocotyl and finally accumulated in the leaves. Following the particles' way upwards from the root into the hypocotyl, we suggest a kind of bottle-neck effect at the transition from the root to the lower hypocotyl (root collar), because the UCNP concentration in the upper hypocotyl is clearly lower in comparison to the root (large UCNPs 190–1000 times; small UCNPs 48–106 times; Fig. 4b) and the root collar (large UCNPs 4–81 times; small UCNPs 5–23 times; Fig. S7, Tables S1 and S2†). This phenomenon can be explained by the deviating anatomical structure of the root collar; exactly here the vascular tissue of the root (actinostele) fans out into the typical vascular tissue of the upper hypocotyl, *i.e.*, the eustele. The LSM data support this preliminary conclusion because they show UCNP emission along the vascular tissue in a longitudinal section of the root collar (Fig. 3). Furthermore, UCNP transport *via* the vascular tissue might be an explanation for the fast translocation of the particles to the cotyledons. The slower cell-by-cell transfer *via* diffusion would not be in accord with our data as we found the first UCNP signals in the cotyledons already 3 h after application of UCNP.[36] After 5 days the particles show a tendency of accumulating at the leave margin where the vascular vessels are ending, while at the lamina their concentrations are about seven (large UCNP) to nine (small UCNP) times lower. So, the fast distribution of UCNP to the cotyledons and the low concentration in the upper hypocotyl together with the LSM data suggest an NP transport *via* the vascular system. It is nevertheless surprising that the larger NP (22 × 41 nm) were taken up and translocated across the whole plant, because the maximum diameter of cell wall pores is approximately 20 nm which should exclude our NPs from crossing cell walls through those pores.[8,45,46] These results support our previous work showing that polydisperse UCNPs bearing HEDP ligands were taken up by orchid plants *via* the cortex and vascular tissue of their aerial roots. The results are also in line with other publications analysing the uptake and distribution potential of differently sized and charged NP on longer timescales of 5–20 days.[9,10,37] In agreement with our results, Zhu *et al.* have shown in experiments with pumpkin plants that Fe_3O_4-NP with particle sizes of 20 nm as well as agglomerates of various sizes (up to 2 μm) accumulate in the roots, the leaves and the root collar.[10] In accordance with our data, the lowest NP concentration was found in the upper region of the shoot. An accumulation of NP at the leaf margin was also observed in a study by Zhang *et al.* using radioactive labelled 7 and 25 nm CeO_2-NP and 24 days old cucumber plants (incubation time 7–14 days).[9] However, they detected a size-dependent accumulation in plant organs resulting in higher concentrations of the 7 nm CeO_2-NP compared to the 25 nm particles. In our study a size-dependent difference in the NP concentration was detected only in the hypocotyl regions and only after five days of incubation. The deviation between our and Zhang's studies could be the difference in the particle sizes used (14 nm and 22 × 41 nm *vs.* 7–25 nm), the different observation times (3 h to 5 days *vs.* 14 days) or the different age of the plants (6–11 days old pumpkin seedlings *vs.* 24 days old cucumber plants). Cells of younger plants are not completely differentiated so the primary cell walls are more flexible and the pores could be stretched to a larger extent.[47]

4 Conclusion

In conclusion, we have shown that nearly monodisperse UCNPs can be used as a multifunctional marker system to investigate the uptake and translocation of nanoparticles in plants. We investigated the kinetics of the nanoparticle uptake for two well-defined particle sizes. Particles of both sizes were taken up and translocated to all plant organs *via* the vascular system within three hours. NP accumulation takes place finally in the leaf margin. The uptake of spherical smaller (14 nm) NP is faster than the uptake of larger 22 × 41 nm NP, leading to higher concentrations of the smaller particles at early times of incubation. This concentration difference, however, decreases with time and the concentration of the different particles becomes very similar in the leaves after 5 days.

Acknowledgements

We thank Mr H. Eickmeier for the TEM investigations, Mrs K. Rücker for assistance with the particle synthesis and Mr R. Grupe for help with the hydroponic set-up.

Notes and references

1 F. Piccinno, F. Gottschalk, S. Seeger and B. Nowack, *J. Nanopart. Res.*, 2012, **14**, 1109.
2 G. Oberdörster, E. Oberdörster and J. Oberdörster, *Environ. Health Perspect.*, 2005, **113**, 823–839.
3 B. Nowack and T. Bucheli, *Environ. Pollut.*, 2007, **150**, 5–22.
4 M. A. Maurer-Jones, I. L. Gunsolus, C. J. Murphy and C. L. Haynes, *Anal. Chem.*, 2013, **85**, 3036–3049.
5 H. Ma, P. L. Williams and S. A. Diamond, *Environ. Pollut.*, 2013, **172**, 76–85.
6 A. Baun, N. B. Hartmann, K. Grieger and K. O. Kusk, *Ecotoxicology*, 2008, **17**, 387–395.
7 O. Bondarenko, K. Juganson, A. Ivask, K. Kasemets, M. Mortimer and A. Kahru, *Arch. Toxicol.*, 2013, **87**, 1181–1200.
8 E. Navarro, A. Baun, R. Behra, N. B. Hartmann, J. Filser, A.-J. Miao, A. Quigg, P. H. Santschi and L. Sigg, *Ecotoxicology*, 2008, **17**, 372–386.
9 Z. Zhang, X. He, H. Zhang, Y. Ma, P. Zhang, Y. Ding and Y. Zhao, *Metallomics*, 2011, **3**, 816.
10 H. Zhu, J. Han, J. Q. Xiao and Y. Jin, *J. Environ. Monit.*, 2008, **10**, 713.
11 X. Ma, J. Geiser-Lee, Y. Deng and A. Kolmakov, *Sci. Total Environ.*, 2010, **408**, 3053–3061.
12 R. Chen, T. A. Ratnikova, M. B. Stone, S. Lin, M. Lard, G. Huang, J. S. Hudson and P. C. Ke, *Small*, 2010, **6**, 612–617.
13 K.-J. Dietz and S. Herth, *Trends Plant Sci.*, 2011, **16**, 582–589.
14 E. Etxeberria, P. Gonzalez, E. Baroja-Fernández and J. P. Romero, *Plant Signaling Behav.*, 2006, **1**, 196–200.
15 W.-M. Lee, Y.-J. An, H. Yoon and H.-S. Kweon, *Environ. Toxicol. Chem.*, 2008, **27**, 1915–1921.
16 D. Lin and B. Xing, *Environ. Sci. Technol.*, 2008, **42**, 5580–5585.
17 R. Nair, A. C. Poulose, Y. Nagaoka, Y. Yoshida, T. Maekawa and D. S. Kumar, *J. Fluoresc.*, 2011, **21**, 2057–2068.
18 C. M. Rico, S. Majumdar, M. Duarte-Gardea, J. R. Peralta-Videa and J. L. Gardea-Torresdey, *J. Agric. Food Chem.*, 2011, **59**, 3485–3498.
19 J. G. Parsons, M. L. Lopez, C. M. Gonzalez, J. R. Peralta-Videa and J. L. Gardea-Torresdey, *Environ. Toxicol. Chem.*, 2010, **29**, 1146–1154.
20 H. Wang, X. Kou, Z. Pei, J. Q. Xiao, X. Shan and B. Xing, *Nanotoxicology*, 2011, **5**, 30–42.
21 M. L. López-Moreno, G. de la Rosa, J. A. Hernández-Viezcas, H. Castillo-Michel, C. E. Botez, J. R. Peralta-Videa and J. L. Gardea-Torresdey, *Environ. Sci. Technol.*, 2010, **44**, 7315–7320.
22 K. Birbaum, R. Brogioli, M. Schellenberg, E. Martinoia, W. J. Stark, D. Günther and L. K. Limbach, *Environ. Sci. Technol.*, 2010, **44**, 8718–8723.
23 S. Asli and P. M. Neumann, *Plant, Cell Environ.*, 2009, **32**, 577–584.
24 S. Lin, J. Reppert, Q. Hu, J. S. Hudson, M. L. Reid, T. A. Ratnikova, A. M. Rao, H. Luo and P. C. Ke, *Small*, 2009, **5**, 1128–1132.
25 R. Doshi, *Environ. Res.*, 2008, **106**, 296–303.
26 R. G. Haverkamp and A. T. Marshall, *J. Nanopart. Res.*, 2009, **11**, 1453–1463.
27 J. Kurepa, T. Paunesku, S. Vogt, H. Arora, B. M. Rabatic, J. Lu, M. B. Wanzer, G. E. Woloschak and J. A. Smalle, *Nano Lett.*, 2010, **10**, 2296–2302.
28 D. Stampoulis, S. K. Sinha and J. C. White, *Environ. Sci. Technol.*, 2009, **43**, 9473–9479.
29 M. Haase and H. Schäfer, *Angew. Chem., Int. Ed.*, 2011, **50**, 5808–5829.
30 D. O. Faulkner, S. Petrov, D. D. Perovic, N. P. Kherani and G. A. Ozin, *J. Mater. Chem.*, 2012, **22**, 24330–24334.
31 J. C. Boyer and F. C. J. M. Van Veggel, *Nanoscale*, 2010, **2**, 1417–1419.
32 S. Wu, G. Han, D. J. Milliron, S. Aloni, V. Altoe, D. V. Talapin, B. E. Cohen and P. J. Schuck, *Proc. Natl. Acad. Sci. U. S. A.*, 2009, **106**, 10917–10921.
33 F. Wang, D. Banerjee, Y. Liu, X. Chen and X. Liu, *Analyst*, 2010, **135**, 1839–1854.
34 J. Zhou, Z. Liu and F. Li, *Chem. Soc. Rev.*, 2012, **41**, 1323.
35 A. Hischemöller, J. Nordmann, P. Ptacek, K. Mummenhoff and M. Haase, *J. Biomed. Nanotechnol.*, 2009, **5**, 278–284.
36 J. Peng, Y. Sun, Q. Liu, Y. Yang, J. Zhou, W. Feng, X. Zhang and F. Li, *Nano Res.*, 2012, **5**, 770–782.
37 Z.-J. Zhu, H. Wang, B. Yan, H. Zheng, Y. Jiang, O. R. Miranda, V. M. Rotello, B. Xing and R. W. Vachet, *Environ. Sci. Technol.*, 2012, **46**, 12391–12398.
38 H.-X. Mai, Y.-W. Zhang, L.-D. Sun and C.-H. Yan, *Chem. Mater.*, 2007, **19**, 4514–4522.
39 H.-X. Mai, Y.-W. Zhang, L.-D. Sun and C.-H. Yan, *J. Phys. Chem. C*, 2007, **111**, 13730–13739.
40 B. Voss and M. Haase, *ACS Nano*, 2013, **7**, 11242–11254.
41 R. Komban, J. P. Klare, B. Voss, J. Nordmann, H.-J. Steinhoff and M. Haase, *Angew. Chem., Int. Ed.*, 2012, **51**, 6506–6510.
42 B. Herden, J. Nordmann, R. Komban, M. Haase and T. Jüstel, *Opt. Mater.*, 2013, **35**, 2062–2067.
43 T. Rinkel, J. Nordmann, A. N. Raj and M. Haase, *Nanoscale*, 2014, **6**, 14523–14530, DOI: 10.1039/c4nr03833a.
44 A. Bresinsky, C. Körner, J. W. Kadereit, G. Neuhaus and U. Sonnewald, *Strasburger Lehrbuch der Botanik*, Spektrum Akad. Verl., Heidelberg, 2008, 36th edn, 1–1071.
45 N. C. Carpita and D. M. Gibeaut, *Plant J.*, 1993, **3**, 1–30.
46 N. Carpita, D. Sabularse, D. Montezinos and D. P. Delmer, *Science*, 1979, **205**, 1144–1147.
47 D. J. Cosgrove, *Nat. Rev. Mol. Cell Biol.*, 2005, **6**, 850–861.

